

Stress Concentration Factors in KT-Joints Subjected to Complex Bending Loads Using Artificial Neural Networks

Mohsin Iqbal ^{1*}, Saravanan Karuppanan ¹, Veeradasan Perumal ¹, Mark Ovinis ², Afzal Khan ³, Muhammad Faizan ⁴

¹ Department of Mechanical Engineering, Universiti Teknologi PETRONAS, Seri Iskandar 32610, Malaysia.

² School of Engineering and the Built Environment, Birmingham City University, Birmingham, United Kingdom.

³ Department of Mechanical Engineering, University of Engineering and Technology, Peshawar 25120, Pakistan.

⁴ Department of Mechanical Engineering, International Islamic University Islamabad, Islamabad, 44000, Pakistan.

Received 20 October 2023; Revised 19 March 2024; Accepted 26 March 2024; Published 01 April 2024

Abstract

Fatigue analysis of tubular joints based on peak stress concentration factor (SCF) is critical for offshore structures as it determines the fatigue life of the joint and possibly the overall structure. It is known that peak SCF occurs at the crown position for in-plane bending (IPB) and at the saddle position for out-of-plane bending (OPB). Tubular joints of offshore structures are under multiplanar bending, comprising IPB and OPB. When a joint is subjected to IPB and OPB loads simultaneously, the peak SCF occurs somewhere between the crown and the saddle. However, existing equations estimate SCF at the crown and saddle only when a joint is subjected to IPB or OPB. It was found that the position and magnitude of peak SCF under simultaneous IPB and OPB depend on the relative magnitudes of these uniplanar load components. The crown and saddle position SCF can be substantially lower than the cumulative peak SCF. Empirical models are proposed for computing peak SCF for KT-joints subjected to multiplanar bending. These models were developed through regression analysis using artificial neural networks (ANN). The ANN training data was generated through 3716 ANSYS finite element simulations. The empirical model was validated using models available in the literature and can determine peak SCF with an error of less than 1.5%.

Keywords: Fatigue Analysis; Stress Concentration Factor; Empirical Modeling; ANN; Multiplanar Bending Load; Tubular KT-Joint.

1. Introduction

Circular hollow section Steel tubular members are preferred for offshore structures due to their high stiffness-to-weight ratio, low drag, and direction-independent structural response. Fatigue due to environmental and operational loads is the primary cause of failure in offshore structures, and it is critical to design for fatigue loading. The weld line at the interface tubular members is typically the most vulnerable to fatigue failure due to stress amplification caused by geometric variation [1, 2], as illustrated in Figure 1. The failure of a joint causes additional load on the neighboring structural elements and can lead to the collapse of the entire structure [3]. Therefore, careful fatigue life estimation is essential for the reliable design of offshore structures [4].

Fatigue life can be estimated experimentally or numerically. Experimental fatigue analysis is usually difficult, costly, and time-consuming. Among various numerical methods, the structural hot-spot stress-based fatigue life estimation is

* Corresponding author: mohsin_22005143@utp.edu.my

 <http://dx.doi.org/10.28991/CEJ-2024-010-04-04>



© 2024 by the authors. Licensee C.E.J, Tehran, Iran. This article is an open access article distributed under the terms and conditions of the Creative Commons Attribution (CC-BY) license (<http://creativecommons.org/licenses/by/4.0/>).

straightforward and widely used when designing offshore structures [4]. This approach is based on fatigue life determination using peak hot-spot stress (HSS) in conjunction with an S-N curve. The HSS in a joint is usually calculated using the stress concentration factor (SCF) and nominal stress, as shown in Equation 1. The nominal stress (σ_n) is the bending stress calculated using beam theory, given by Equation 2 [5].

$$\sigma_{HSS} = SCF * \sigma_n \quad (1)$$

$$\sigma_n = \frac{32 d M}{\pi[d^4 - (d-2t)^4]} \quad (2)$$

where σ_{HSS} is hot-spot stress (HSS), SCF is stress concentration factor, σ_n is nominal stress in the brace, d is diameter of the brace, M is moment on the brace, t is brace wall thickness.

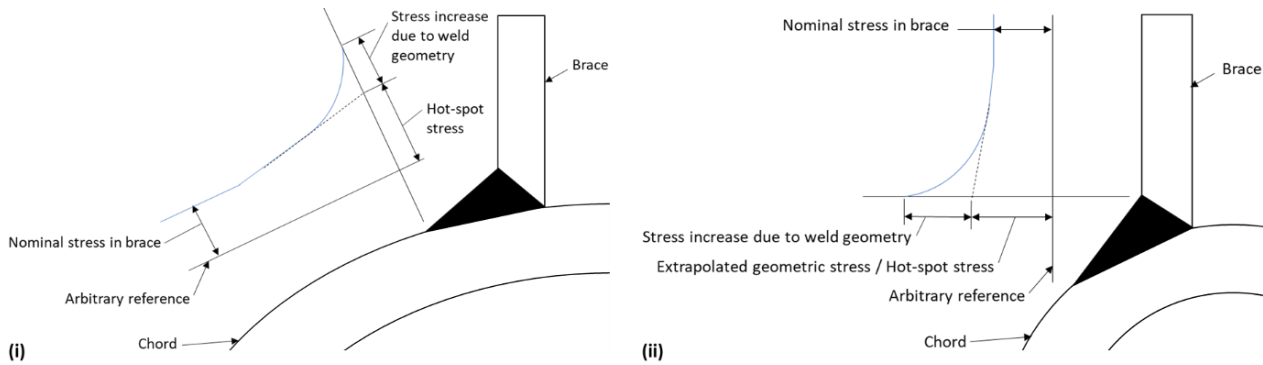


Figure 1. Stress amplification at tubular joints: (i) chord-side of the interface, (ii) brace-side of the interface

The SCF measures stress amplification at a tubular joint and depends on the geometry and load on the joint. Significant efforts have been devoted to investigating and developing empirical models for SCF in various tubular joints. These studies can be traced back to Kuang et al. [6], Wordsworth [7], Wordsworth and Smedley [8], Efthymiou [9], Hellier et al. [10], Lloyd [11], Smedley and Fisher [12], and Morgan et al. [13, 14]. Efthymiou's equations [9] are widely used for estimating the fatigue life of KT-joint and are included in various standards such as DNV-GL-RP203 [15], NORSOK [16], and CIDECT [17]. The geometric configurations and load conditions of KT-joints are varied, and numerous aspects have been actively explored in recent years. Many researchers have investigated SCF concerning different design aspects of KT joints subjected to bending and proposed numerical models to determine SCF rapidly.

Ahmadi & Zavvar [18] investigated KT-joints with internal ring stiffeners under four different configurations of OPB and proposed empirical models for determining SCF at the saddle positions. They conducted a study [19] in which four different IPB load conditions were investigated using 118 finite element (FE) models, and empirical models were developed for the crown position of the central brace and the toe of inclined braces. Simulations of these two studies [18, 19] could be used to determine the combined SCF effect of IPB and OPB using the superposition of stress. However, while the peak SCF of simultaneous loads occurs somewhere between crown and saddle, the empirical models were only for SCF at the saddle for OPB and the crown for IPB. Utilizing these models will underestimate the peak SCF. Therefore, empirical models that can estimate SCF around the brace axis are required. Additionally, they investigated the probability distribution functions for SCFs in internal ring-stiffened KT-joints under IPB [20]. Four IPB load configurations were explored using 108 simulations. Various probability density functions (PDFs) were fitted to the maximum SCFs, and the goodness of fit was evaluated using Kolmogorov-Smirnov and chi-squared tests. These investigations were limited to SCF to locations of maximum SCF when the KT-joint is subjected to either IPB or OPB. They simulated 432 FE models of KT-joint under various OPB loads and investigated the probability distribution of SCF at saddle position [21] under various configurations of IPB loads. Ten parametric equations were proposed for determining SCFs at braces' crown, toe, and heel positions by regression analysis of data obtained through 46 simulations [22]. They also investigated the effect of multilinearity by stimulating 81 finite models [23]. It was found that the SCF in multiplanar joints can be substantially higher than in uniplanar KT-joints. However, SCF equations were only available for uniplanar KT-joints under IPB and OPB, and using these parametric models for multiplanar joints would underestimate the SCF.

New empirical models were proposed for multiplanar KT-joints under bending. However, both the old and new models were only for determining SCF at saddle and crown positions. These models are valid when a joint is subjected to either IPB or OPB, but not both. Zavvar et al. [24] investigated the SCF of uniplanar and multiplanar KT-joints subjected to IPB. Four IPB load configurations were investigated through 81 FE simulations. Empirical models were

proposed for determining SCF at the crown position. They also investigated SCF in FRP-reinforced KT- joints under IPB and OPB [25]. Simulation of 2920 FE models was carried out, and 38 parametric equations were proposed for determining SCF at the crown and saddle of the central brace while at the heel and toe of inclined braces. All existing models are limited to determining SCF at specific locations, as outlined in Table 1. None of these models can determine SCF around the brace axis for a joint subjected to simultaneous in-plane bending (IPB) and out-of-plane bending (OPB).

Table 1. Literature on empirical modeling of SCF in KT-joint under bending loads

S. No.	Article	Ref. No.	Joint	Load	Empirical model
1.	Development of SCF formulae and generalized influence functions for use in fatigue analysis (1988).	[9]	KT-joint (base model)	IPB, OPB (not simultaneous)	Equations were proposed for determining the SCF at the joint crown for IPB and the saddle for OPB.
2.	Stress concentration factors induced by out-of-plane bending loads in ring-stiffened tubular KT-joints of jacket structures (2015).	[18]	KT-joint with internal ring stiffeners	OPB	Empirical models were developed for the SCF at joint saddle under four OPB configurations.
3.	Stress concentration due to in-plane bending (IPB) loads in ring-stiffened tubular KT-joints of offshore structures: parametric study and design formulation (2015).	[19]	KT-joint with internal ring stiffeners	IPB	Empirical models were developed for the SCF at the joint crown under four OPB configurations.
4.	Probabilistic analysis of stress concentration factors in tubular KT-joints reinforced with internal ring stiffeners under in-plane bending loads (2015).	[20]	KT-joint with internal ring stiffeners	IPB	The best-fit probability distribution function was identified for the SCF at the joint crown joint under IPB.
5.	A probability distribution model for SCFs in internally ring-stiffened tubular KT-joints of offshore structures subjected to out-of-plane bending loads (2016).	[21]	KT-joint with internal ring stiffeners	OPB	The best-fit probability distribution function was identified for the SCF at the joint crown.
6.	Stress concentration factors in uniplanar tubular KT-joints of jacket structures subjected to in-plane bending loads (2016).	[22]	KT-joint (base model)	IPB	Ten parametric equations were proposed to determine the SCFs at crown of the central brace, and toe and heel of the outer braces.
7.	The effect of multi-planarity on the SCFs in offshore tubular KT-joints subjected to in-plane and out-of-plane bending loads (2016).	[23]	Uniplanar, and multiplanar KT-joint	IPB, OPB (not simultaneous)	Empirical models were proposed for the SCF at the joint crown for IPB and joint saddle for OPB.
8.	Stress concentration factors of multiplanar tubular KT-joints subjected to in-plane bending moments (2021).	[24]	Uniplanar, and multiplanar KT-joint	IPB	Empirical models were proposed for the SCF at crown of uniplanar and multiplanar KT-joint subjected to IPB.
9.	Stress concentration factors in steel tubular KT-connections with FRP-Wrapping under bending moments (2021).	[25]	FRP reinforced KT-joint	IPB, OPB (not simultaneous)	Parametric equations were proposed for the SCF at the central brace crown and saddle at the heel and toe of inclined braces.
10.	Empirical modeling of stress concentration factors using finite element analysis and artificial neural networks for the fatigue design of tubular KT-joints under combined loading (2023).	[26]	KT-joint (base model)	Axial, IPB, OPB (individual and simultaneous load on central brace only)	Empirical models were presented for the SCF around the axis of the central brace. (including the crown and saddle positions)

Fatigue life estimation is based on the peak SCF and S-N curves. The peak SCF occurs at the crown position when a joint is subjected to IPB, while at the saddle position when it is subjected to OPB. Therefore, while the empirical models are available for IPB and OPB, no models are available when a joint is subjected to multiplanar bending loads, e.g., simultaneous IPB and OPB, as the location of peak SCF varies between the crown and saddle [27]. The peak HSS for joints subjected to combined loads depends on the magnitudes and directions of the load components [28]. In such cases, HSS can be determined by the superposition of stress due to uniplanar load components by determining SCF around the brace axis, superimposing it to find the peak HSS, and calculating fatigue life. However, none of the available empirical models can determine SCF around the brace axis. Recently, Iqbal et al. [26] proposed empirical models capable of determining SCF around the brace axis of a KT-joint; however, only the central brace was subjected to bending loads. In this work, the SCF around the brace axis for the KT-joint is investigated, with all braces subjected to bending. 3716 numerical simulations were carried out, and the results generated were used to develop empirical models. These models were validated with finite element simulations and existing equations.

2. Simulation of KT-joint under Bending Loads

This study investigates KT-joints subjected to bending. FE models of KT-joints were simulated using the static structural module of ANSYS. Artificial neural network (ANN) models were trained using finite element analysis (FEA), and empirical models were developed. The methodology is summarized in Figure 2.

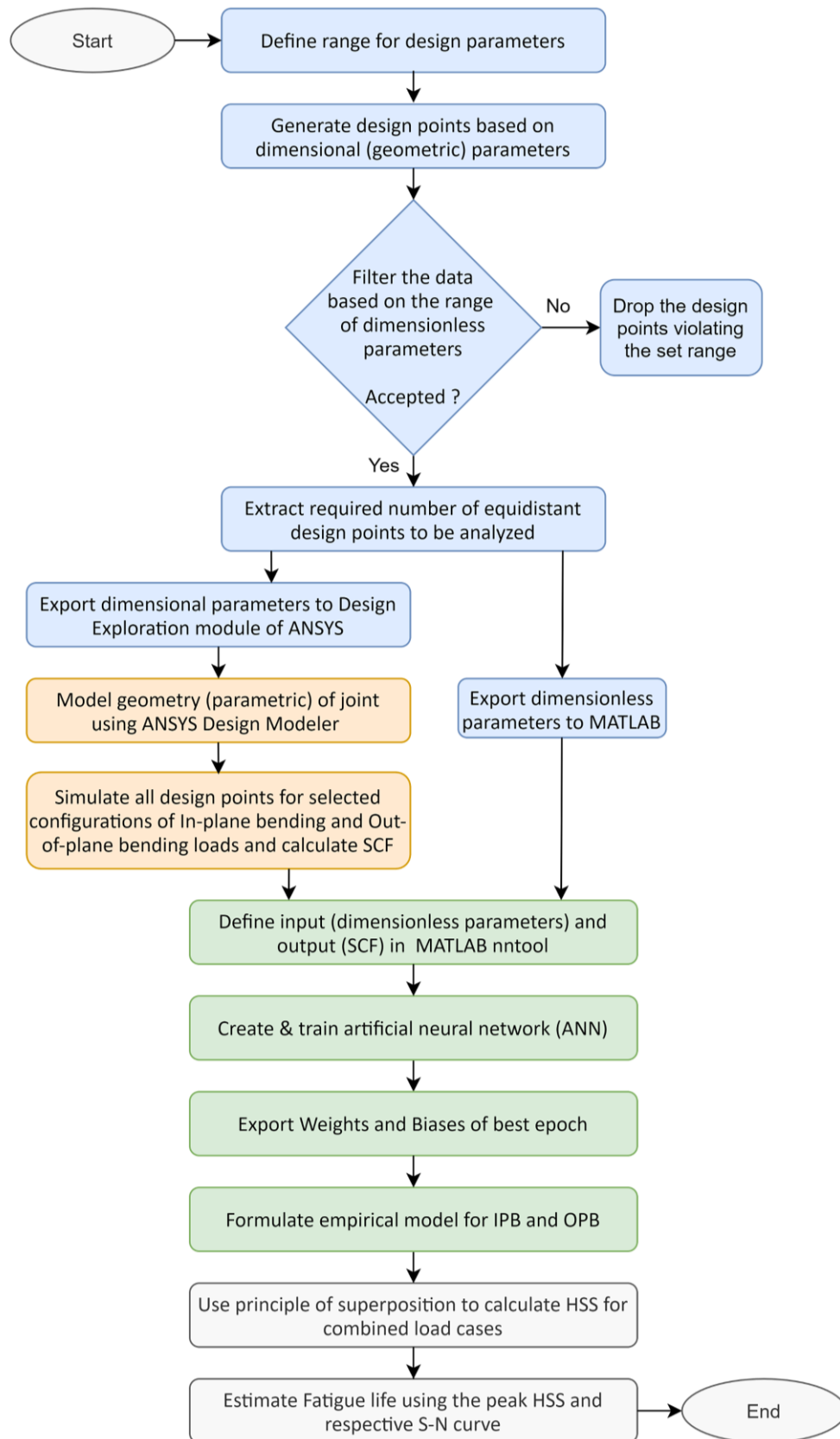


Figure 2. Methodology for determining the SCF in KT-joint under bending

The KT-joint was defined as a function of dimensionless parameters $\beta, \gamma, \tau, \theta, \alpha,$ and ζ , given in Equations 3-7. The range for these parameters is listed in Table 2. The design data set was generated based on the equidistance distribution of variables $D, d, T, t, \theta,$ and g . This initial set of design points was generated using the permutation dimensionless parameters. Some of these data points were violating the range defined. Design points outside the range of dimensionless parameters were excluded. Due to the continuous nature of all dimensionless parameters, the design data set could

contain infinite design points, which need to be limited for simulation in due time. Pre-set data points were selected from this data, ensuring this selection was equally distributed around the initial data set and simulated using ANSYS, following the steps shown in Figure 2.

$$\tau = t/T \tag{3}$$

$$\gamma = D/2T \tag{4}$$

$$\alpha = 2L/D \tag{5}$$

$$\zeta = g/D \tag{6}$$

$$\beta = d/D \tag{7}$$

where D is diameter of chord, d is diameter of brace (all), T is chord wall thickness, t is brace wall thickness (all), L is chord length, g is gap b/w central and inclined braces at the chord surface.

Table 2. Range for the parameters used [26]

Type	Parameters	Range	Reference
Derived Parameters (dimensionless)	τ	0.3–0.7	ARSEM Guide [29]
	γ	12–20	ARSEM Guide [29]
	α	5–40	Lloyd's Register [12], ISO Guide [30]
	ζ	0.25–0.5	Ahmadi et al. [18, 31], Ahmadi [32]
	β	0.4–0.8	ARSEM Guide [29]
Geometric Parameters	θ	30–75°	ARSEM Guide [29]
	g	100 (mm)	Ahmadi [32]
	L	1800–3000 (mm)	α_{max} , D_{max} , α_{min} , and D_{min}
	t	3–10 (mm)	Manufacturing limit (assumption)
	T	3–10 (mm)	Manufacturing limit (assumption)
	d	80–320 (mm)	β_{max} , D_{min} , and D_{max}
	D	200–400 (mm)	$D \geq 150$ (Lloyd's Register [12]), γ_{max} and T_{max}

The 3D model of the KT-joint was generated using ANSYS Design Modeler. Geometric inputs were assigned as parametric variables. The joint geometry was meshed using high-order nonlinear elements, as shown in Figure 3-a. A mesh with 223630 elements was used following a sensitivity study. This model was validated with results by Ahmadi et al. [20], as presented in Figure 3-b, with a difference of less than 3% for the numerical model. However, the difference with the experimental results was 15%, possibly due to approximations in the sizing of joints used. The numerical results are usually based on the nominal wall thickness, and a difference in nominal wall thickness and measured wall thickness would cause a mismatch between the numerical and experimental results [33]. This validated model was used for further investigations.

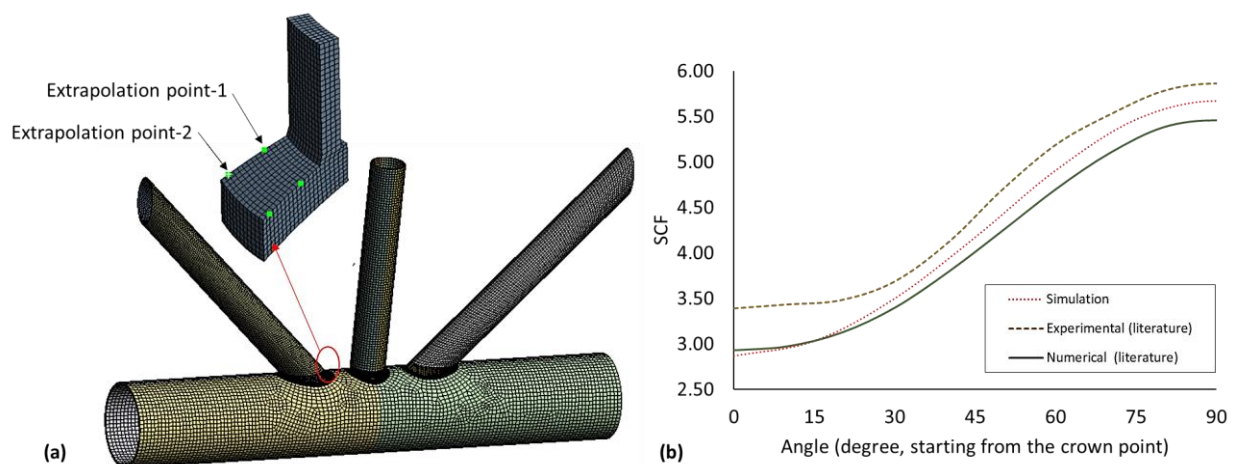


Figure 3. FE model of KT-joint: (a) finite element model, (b) validation of finite element model with the literature [24]

Simulation of 929 geometric design configurations of KT-joints was carried out using ANSYS for each of the four bending configurations, as shown in Figure 4. The first two loadings are IPB, and the latter two are OPB. Bending on a typical KT-joint can be either of these cases or a combination of an IPB and OPB. The chord ends were constrained in all degrees of freedom (three displacements and three rotations), and static structural analysis was performed. Linear elastic simulations are reasonable for determining SCF in tubular joints [34, 35].

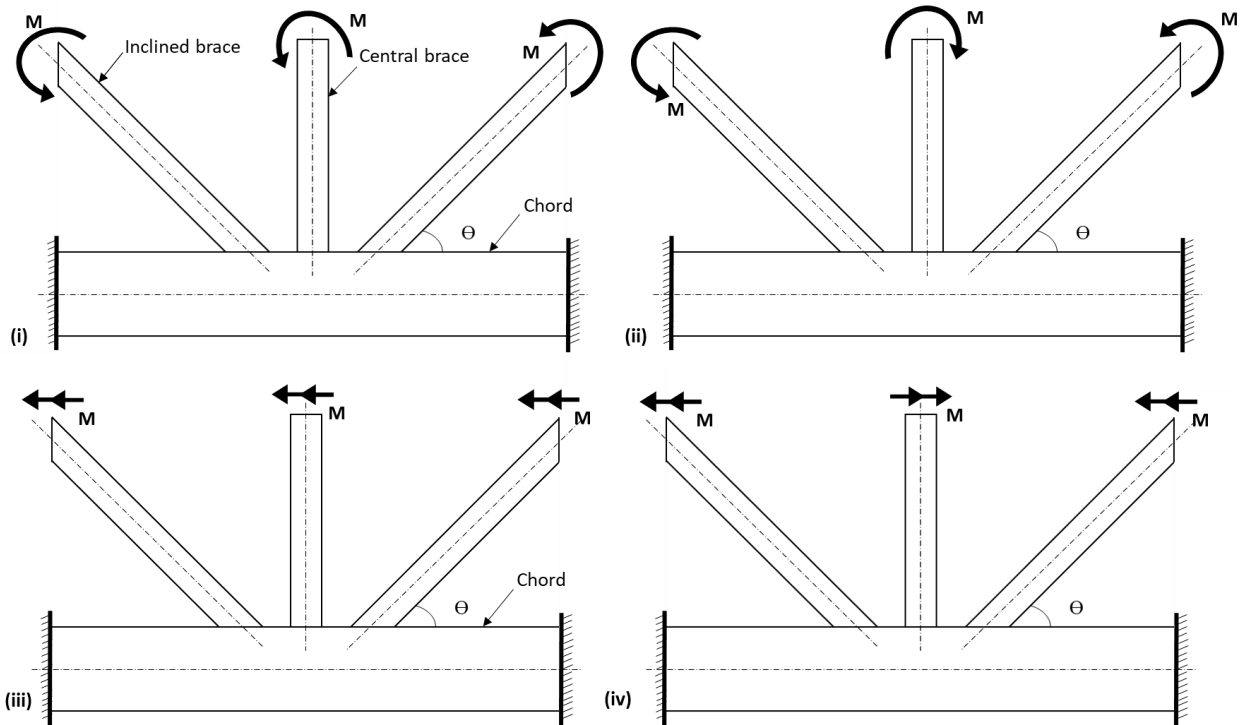


Figure 4. KT-joint subjected to brace bending loads: (i) in-plane bending condition-1, (ii) in-plane bending condition-2, (iii) out-of-plane bending condition-1, (iv) out-of-plane bending condition-2

A Python code was integrated into the ANSYS to automate the determination and extrapolation of stress. This code extracts the stress and position coordinates of the reference points and computes the stress at the weld toe using linear extrapolation. Twenty-four positions were selected to determine stress around the brace axis, as shown in Figure 5-a. For gapped CHS, the variation in stress near the weld toe is almost linear [33]; hence, linear extrapolation was used, as illustrated in Figure 5-b. This extrapolated stress at the weld toe is referred to as HSS. This stress is expressed as a dimensionless parameter (SCF) using Equation 1. Various finite element models were simulated, and SCF was recorded for each simulation. This data was used for regression analysis to develop empirical models for the SCF.

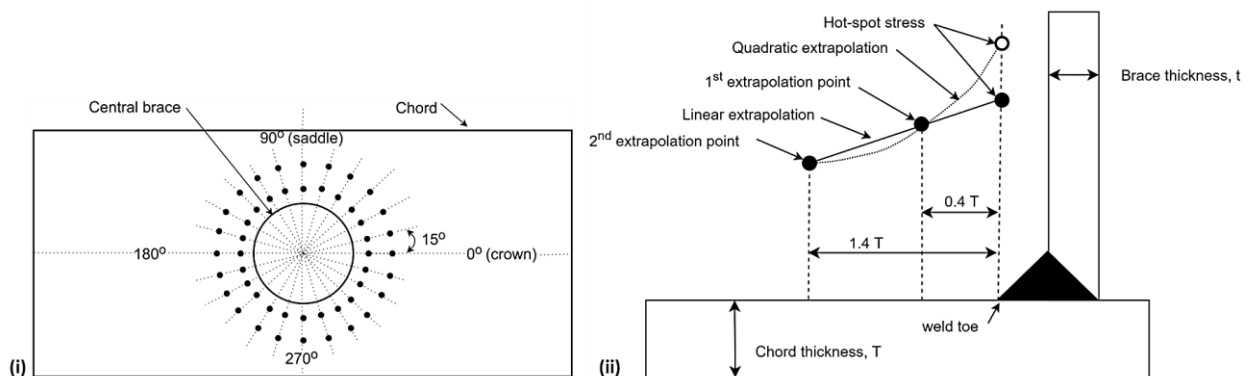


Figure 5. Stress extrapolation: (i) Stress extraction points, (ii) linear extrapolation of principal stress

3. Development and Training of Artificial Neural Networks

An ANN was constructed using MATLAB's tool, as illustrated in Figure 6. The dimensionless parameters served as the inputs, and the SCF along the weld toe of the central brace were the outputs for ANN. Various combinations of hidden layers and neurons were compared, and finally, a configuration with one hidden layer with ten neurons was used

to model the ANN. The Levenberg–Marquardt backpropagation algorithm was applied [36], and the ANN model was trained using the data generated from the FEA with a coefficient of determination $R^2 > 0.999$ and the mean squared error < 0.01 . The regression and performance plots of the training process are shown in Figures 7 and 8. The inputs to empirical expression are normalized to avoid the dominance of a variable with larger magnitudes. The output will be denormalized after calculation. The equations for normalization and denormalization are given as Equations 8 and 9.

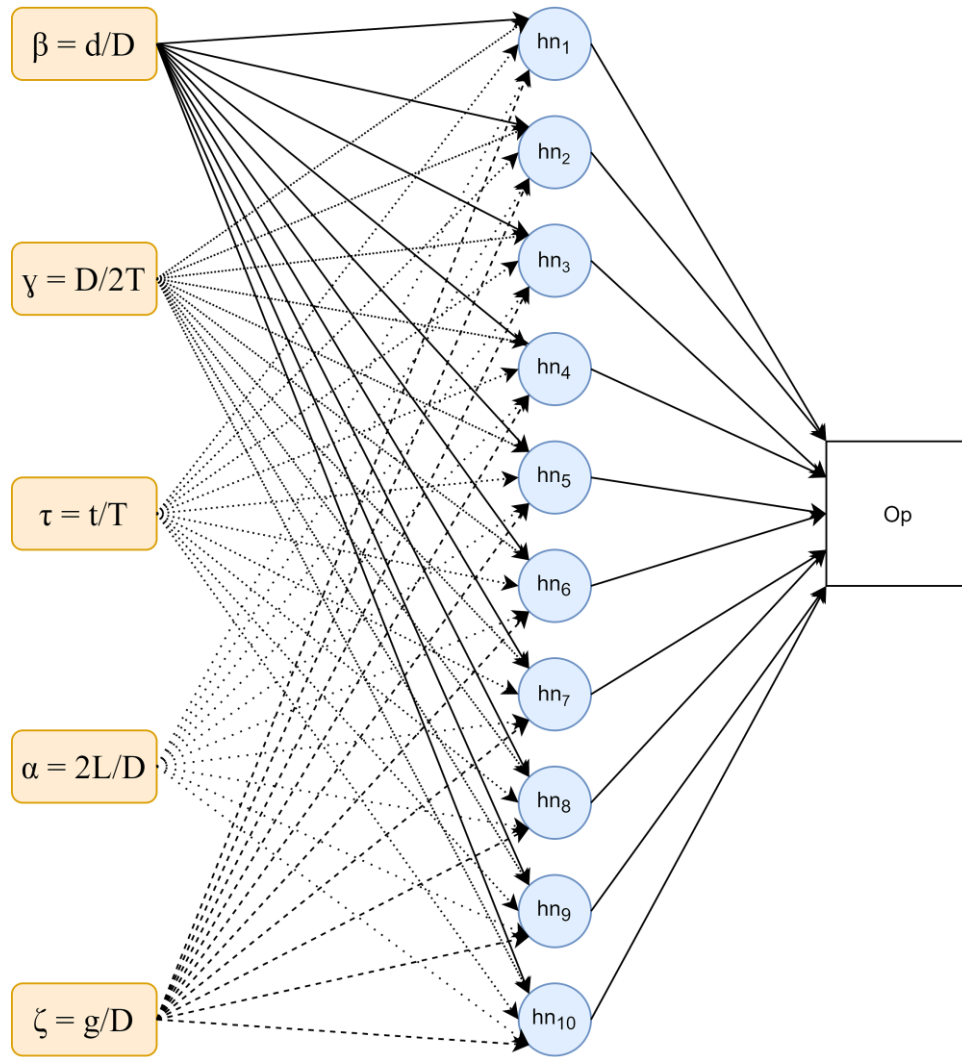
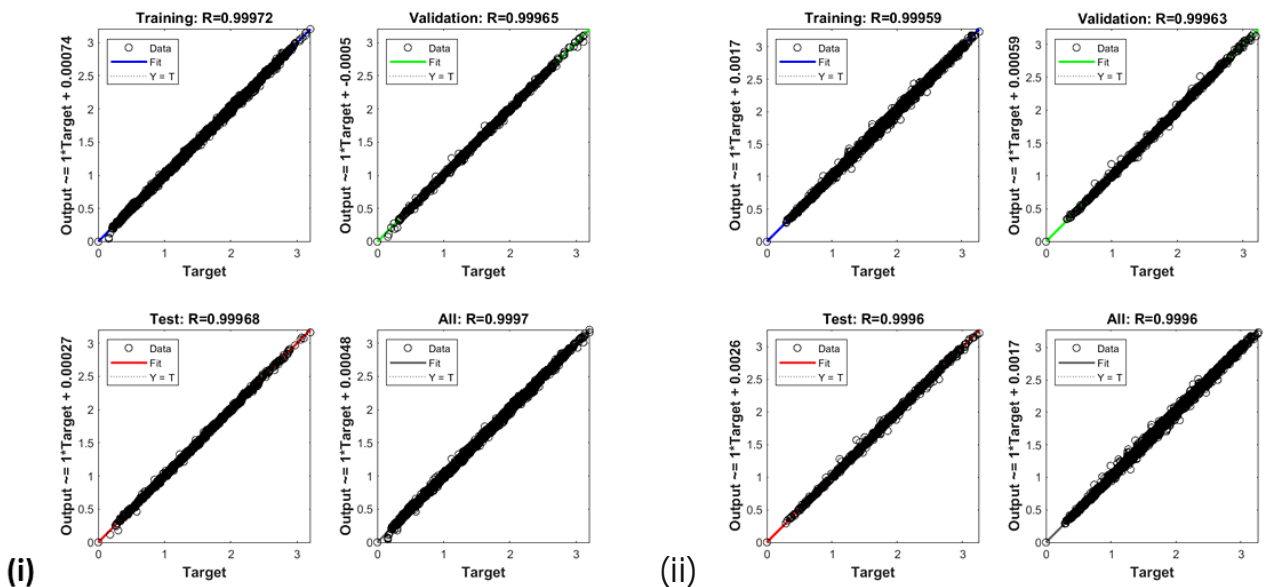


Figure 6. The artificial neural network model



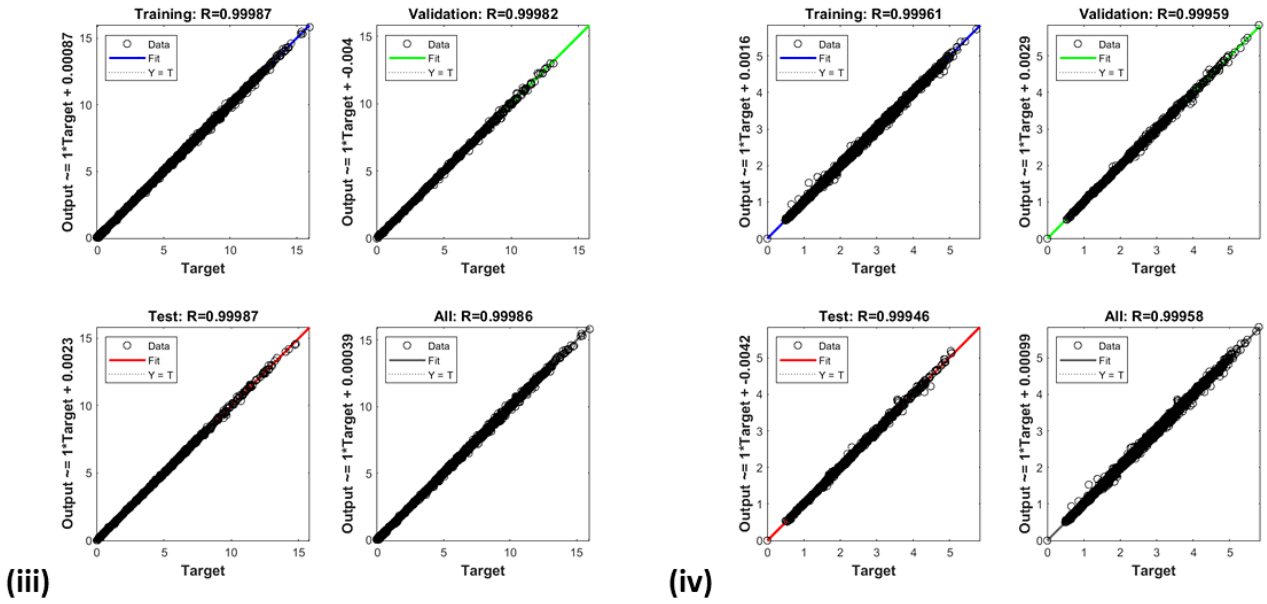


Figure 7. Regression plots: (i) in-plane bending condition-1, (ii) in-plane bending condition-2, (iii) out-of-plane bending condition-1, (iv) out-of-plane bending condition-2

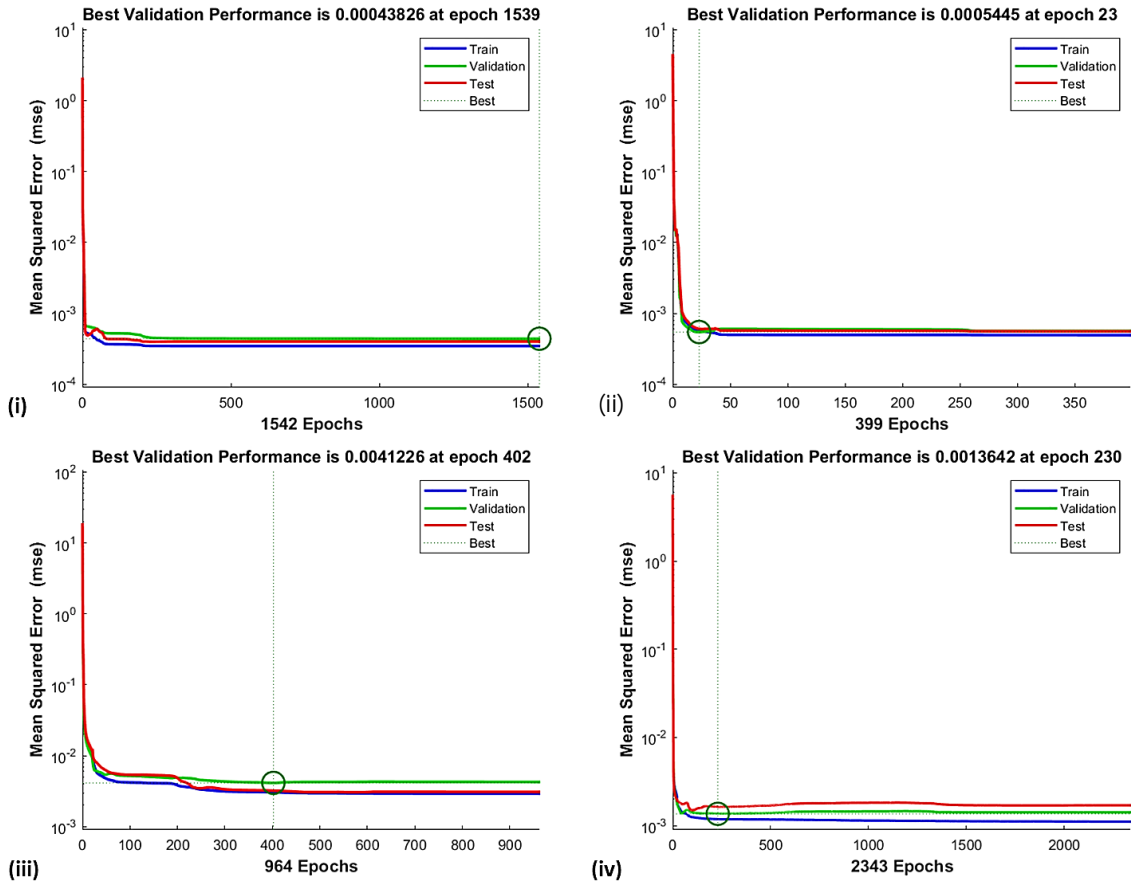


Figure 8. Performance plots: (i) in-plane bending condition-1, (ii) in-plane bending condition-2, (iii) out-of-plane bending condition-1, (iv) out-of-plane bending condition-2

$$i_{normalized} = \frac{(i_{n,max} - i_{n,min})(i - i_{min})}{(i_{max} - i_{min})} + i_{n,min} \tag{8}$$

$$o_{denormalized} = \frac{(o_n - o_{n,min})(o_{max} - o_{min})}{(o_{n,max} - o_{n,min})} + o_{min} \tag{9}$$

where $i_{n,max}$ is 1, i_{max} is max value in input data, $i_{n,min}$ is -1, i_{min} is min value in input data, $o_{n,max}$ is 1, o_{max} is max value of SCF is simulation results, $o_{n,min}$ is -1, o_{min} is min value of SCF in simulation results.

IPB and OPB cases were individually simulated, and ANN was trained for each case. The weights and biases of the trained model were employed for the mathematical modeling of SCF. Stress can be superimposed on IPB and OPB when the joint material remains in the linear elastic range [5, 13, 37]. The combined HSS was computed using Equation 10. The results determined are discussed in the next section.

$$Peak\ HSS = SCF_{ipb}\sigma_{nominal\ ipb} + SCF_{opb}\sigma_{nominal\ opb} \tag{10}$$

4. Empirical Modeling of Stress Concentration Factors

The equations for the SCF in KT-joint subjected to simultaneous brace bending were developed for four configurations applied individually. Two of these represent IPB, and the other two represent OPB. A typical complex bending load can be resolved into IPB and OPB components. For individual load cases, the other component will have null magnitude. Empirical models were developed for each case, and their effect was linearly superimposed using Equation 10. These models were validated with detailed FEA for individual and combined load cases. Empirical equations were developed for quarter geometry (1/4th), with the other quarter having an inverted SCF and the remaining half being symmetric. Equations 15-22 have been developed for SCF along the weld toe of the central brace. The SCF determined through these ANN-based equations was validated through finite element analysis of different KT-joint designs. The SCFs for nine randomly selected designs are shown in Figures 9 to 15. The maximum error in the SCF was 4.7, 4.0, 3.3, and 4.9% for IPB_C1, IPB_C2, OPB_C1 and OPB_C2, respectively. These nine designs were other than those used for training the ANN model, as presented in Table 3.

$$SCF_{chord_crown} = 1.45 \beta \tau^{0.85} \gamma^{(1-0.68\beta)} \sin \theta \tag{11}$$

$$SCF_{chord-saddle} = T_B [1 - 0.8(\beta_A \gamma)^{0.5} \exp(-0.8x_{AB})]^{(\beta_A/\beta_B)^2} \cdot [1 - 0.8(\beta_C \gamma)^{0.5} \exp(-0.8x_{BC})]^{(\beta_C/\beta_B)^2} + T_A [1 - 0.8(\beta_B \gamma)^{0.5} \exp(-0.8x_{AB})] \cdot [2.05(\beta_{max})^{0.5} \exp(-1.3x_{AB})] + T_C [1 - 0.8(\beta_B \gamma)^{0.5} \exp(-0.8x_{BC})] \cdot [2.05(\beta_{max})^{0.5} \exp(-1.3x_{BC})]$$

$$T_i = \gamma \tau_i \beta_A (1.7 - 1.05\beta_i^3) \sin^{1.8} \theta_i \tag{12}$$

where $i = A, B, C$ (inclined brace 1, central brace and inclined brace 2)

$$X_{AB} = 1 + \frac{\zeta_{AB} \sin \theta_B}{\beta_B}$$

$$X_{BC} = 1 + \frac{\zeta_{BC} \sin \theta_B}{\beta_B}$$

$$SCF_{crown} = 0.566 \tau^{0.883} \gamma^{0.715} \beta^{-0.003} \theta^{0.061} \tag{13}$$

$$SCF_{crown} = 0.671 \tau^{0.848} \gamma^{0.683} \beta^{0.115} \theta^{0.023} \tag{14}$$

$$\begin{bmatrix} h_1 \\ h_2 \\ h_3 \\ h_4 \\ h_5 \\ h_6 \\ h_7 \\ h_8 \end{bmatrix} = \begin{bmatrix} 0.04 & 0.04 & 0.29 & 0.26 & 0.06 & -0.46 \\ 0.14 & 0.28 & -0.04 & -0.04 & 0.00 & -0.15 \\ -0.80 & 0.13 & -0.14 & -0.01 & 0.01 & -0.05 \\ 0.14 & 0.27 & -0.04 & -0.04 & 0.00 & -0.15 \\ 0.78 & 0.04 & -0.26 & -0.07 & -1.58 & -0.13 \\ -2.51 & -0.71 & 0.83 & 2.17 & 3.27 & -0.14 \\ -0.31 & 0.14 & 0.35 & -0.01 & -0.04 & 0.25 \\ -0.76 & -0.03 & 0.26 & 0.05 & 1.56 & 0.15 \\ 0.82 & 0.10 & 0.36 & 0.05 & 0.00 & -0.15 \\ 0.82 & 0.10 & 0.36 & 0.05 & 0.00 & -0.15 \end{bmatrix} \begin{bmatrix} \beta_n \\ \gamma_n \\ \tau_n \\ \theta_n \\ \alpha_n \\ \zeta_n \end{bmatrix} + \begin{bmatrix} -1.80 \\ -0.80 \\ 1.39 \\ -0.80 \\ -4.12 \\ 2.64 \\ -0.10 \\ 4.62 \\ 0.15 \\ 0.16 \end{bmatrix} \tag{15}$$

$$\begin{bmatrix} SCF_0 \\ SCF_{15} \\ SCF_{30} \\ SCF_{45} \\ SCF_{60} \\ SCF_{75} \\ SCF_{90} \end{bmatrix} = \begin{bmatrix} 1.63 & -64.27 & 0.08 & 66.61 & 124.42 & 0.04 & 0.60 & 335.10 & -22.04 & 22.52 \\ 1.06 & -74.73 & 0.09 & 77.43 & 47.62 & 0.01 & 0.63 & 127.79 & -24.15 & 24.64 \\ -0.01 & -85.26 & 0.25 & 88.26 & -86.94 & -0.04 & 0.54 & -234.45 & -23.93 & 24.40 \\ -0.55 & -82.97 & 0.41 & 85.92 & -147.43 & -0.06 & 0.44 & -396.42 & -17.20 & 17.59 \\ -0.64 & -87.33 & 0.60 & 90.56 & -164.13 & -0.06 & 0.41 & -440.50 & -10.99 & 11.33 \\ -0.53 & -96.41 & 1.21 & 100.15 & -147.90 & -0.05 & 0.51 & -398.90 & 3.11 & -2.82 \\ 0.49 & -78.73 & -1.89 & 82.40 & 200.67 & 0.11 & 1.31 & 542.80 & 175.02 & -175.93 \end{bmatrix} \begin{bmatrix} h_1 \\ h_2 \\ h_3 \\ h_4 \\ h_5 \\ h_6 \\ h_7 \\ h_8 \end{bmatrix} + \begin{bmatrix} -207.78 \\ -77.46 \\ 149.43 \\ 250.35 \\ 277.68 \\ 252.14 \\ -337.24 \end{bmatrix} \tag{16}$$

$$\begin{bmatrix} h_1 \\ h_2 \\ h_3 \\ h_4 \\ h_5 \\ h_6 \\ h_7 \\ h_8 \\ h_9 \\ h_{10} \end{bmatrix} = \begin{bmatrix} -0.29 & -1.29 & -0.14 & 0.71 & 0.48 & 0.14 \\ -0.11 & -0.40 & 0.55 & -0.02 & 0.01 & 0.04 \\ 1.36 & 0.36 & -0.37 & -0.80 & -2.26 & -0.14 \\ -1.36 & 0.14 & -0.22 & 0.01 & 0.00 & -0.03 \\ 0.20 & 0.27 & 0.30 & 0.01 & 0.00 & -0.07 \\ -0.81 & -0.58 & -0.21 & -0.31 & -0.36 & 0.56 \\ -0.69 & -0.16 & -0.37 & 0.04 & 0.07 & 0.25 \\ 0.64 & -0.02 & -0.18 & -0.08 & -0.10 & -0.14 \\ -0.77 & -0.28 & 0.05 & 0.05 & 0.12 & 0.17 \\ 0.13 & 0.31 & 0.50 & 0.01 & -0.02 & -0.24 \end{bmatrix} \begin{bmatrix} \beta_n \\ \gamma_n \\ \tau_n \\ \theta_n \\ \alpha_n \\ \zeta_n \end{bmatrix} + \begin{bmatrix} -2.02 \\ 0.65 \\ -4.02 \\ 1.53 \\ 0.23 \\ 0.50 \\ -0.64 \\ 0.02 \\ -0.46 \\ -1.05 \end{bmatrix} \tag{17}$$

$$\begin{bmatrix} SCF_0 \\ SCF_{15} \\ SCF_{30} \\ SCF_{45} \\ SCF_{60} \\ SCF_{75} \\ SCF_{90} \end{bmatrix} = \begin{bmatrix} -0.01 & 0.39 & -0.44 & 0.07 & 1.14 & 0.10 & -0.10 & -0.02 & 0.17 & 0.71 \\ -0.02 & 0.44 & -0.23 & 0.08 & 1.08 & 0.09 & -0.15 & -0.25 & 0.07 & 0.74 \\ -0.03 & 0.47 & 0.34 & 0.09 & 0.64 & 0.05 & -0.29 & -0.81 & -0.33 & 0.65 \\ -0.03 & 0.54 & 0.61 & 0.18 & 0.59 & -0.02 & -0.13 & -0.89 & -0.56 & 0.63 \\ -0.03 & 0.53 & 0.58 & 0.28 & 0.66 & -0.06 & 0.07 & -0.73 & -0.60 & 0.75 \\ -0.01 & 0.60 & 0.40 & 0.69 & 0.89 & -0.11 & 0.33 & -0.27 & -0.51 & 0.71 \end{bmatrix} \begin{bmatrix} h_1 \\ h_2 \\ h_3 \\ h_4 \\ h_5 \\ h_6 \\ h_7 \\ h_8 \\ h_9 \\ h_{10} \end{bmatrix} + \begin{bmatrix} -0.47 \\ -0.41 \\ -0.09 \\ 0.05 \\ 0.08 \\ -0.42 \end{bmatrix} \quad (18)$$

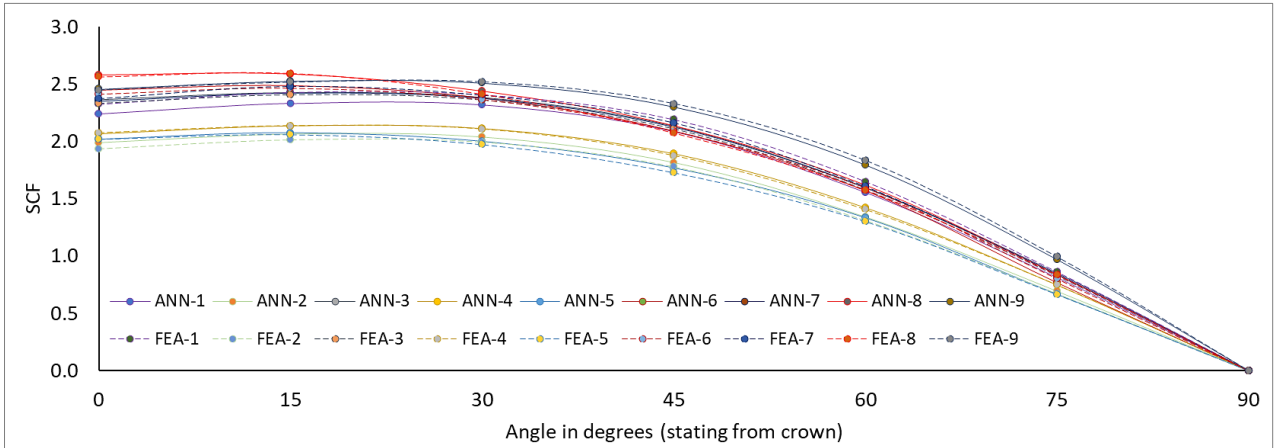


Figure 9. Comparison of stress concentration factor for in-plane bending condition-1 determined using empirical model and finite element analysis

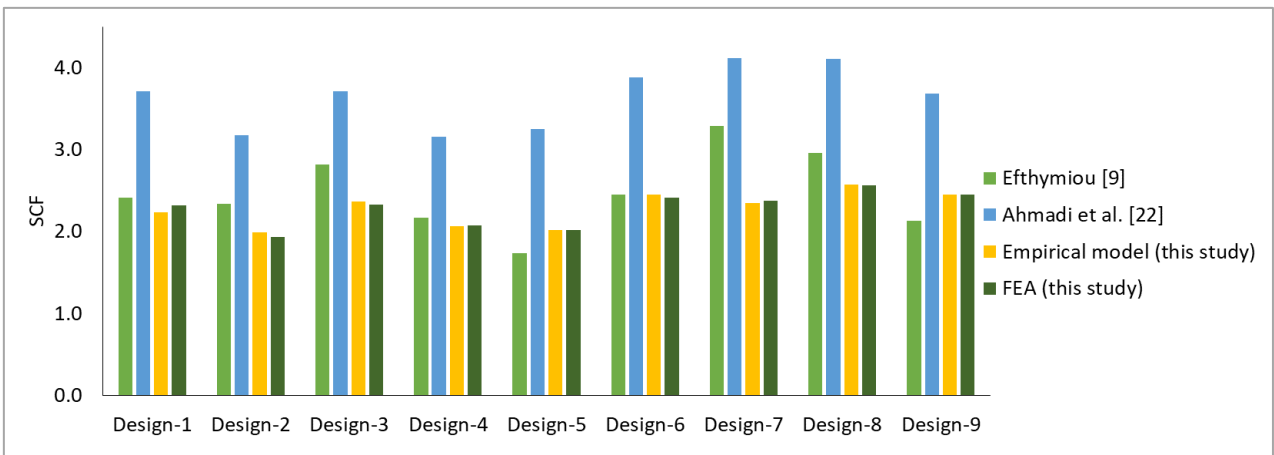


Figure 10. Comparison of stress concentration factor determined using Equations 15 and 16 to existing models

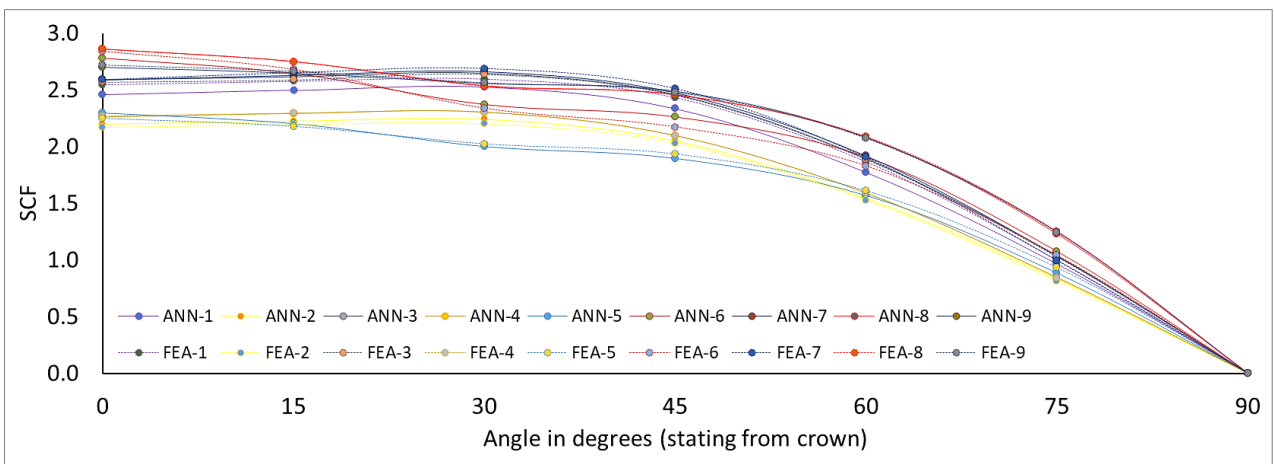


Figure 11. Comparison of stress concentration factor for in-plane bending condition-2 determined using empirical model and finite element analysis

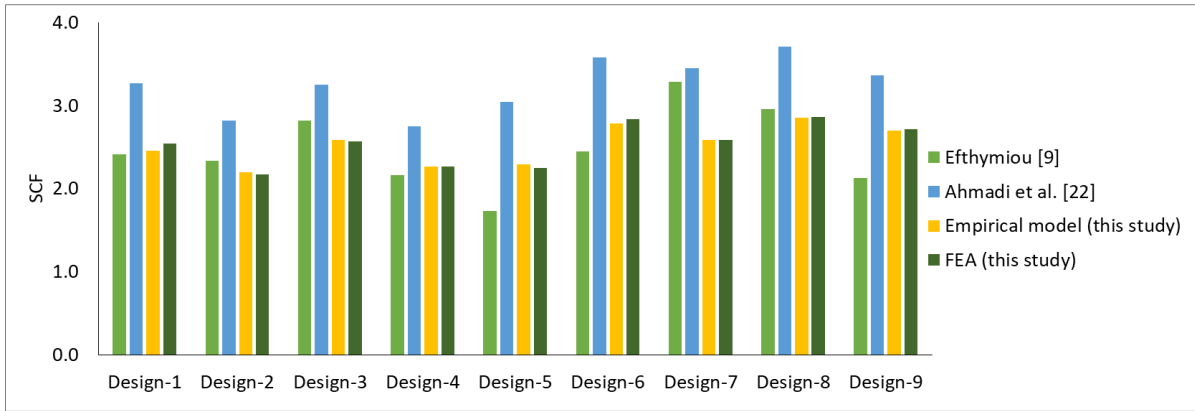


Figure 12. Comparison of stress concentration factor determined using Equations 17 and 18 to existing models

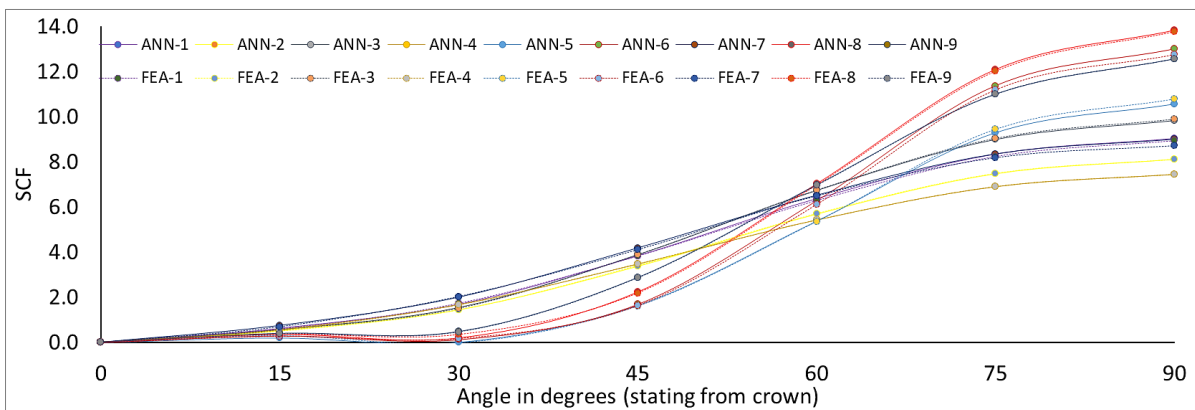


Figure 13. Comparison of stress concentration factor for out-of-plane bending condition-1 determined using empirical model and finite element analysis

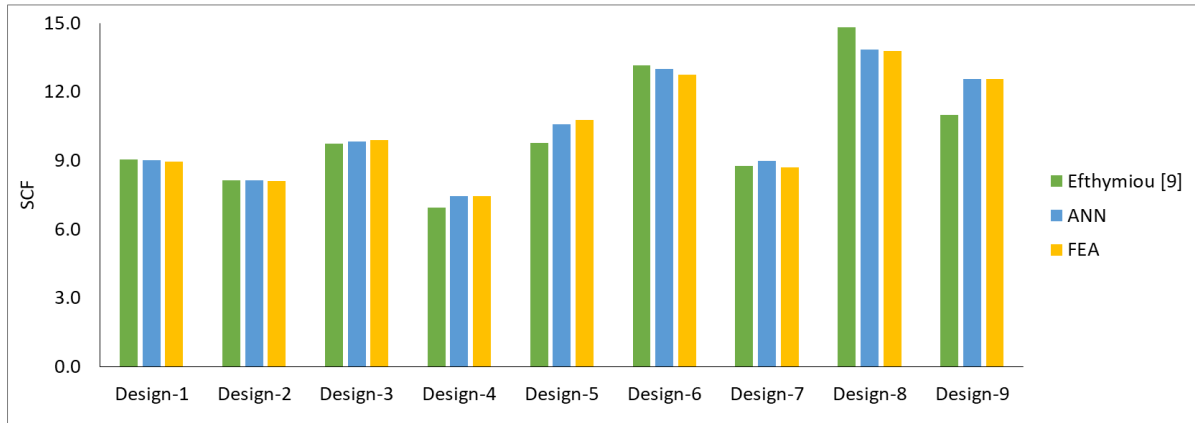


Figure 14. Comparison of stress concentration factor determined using Equations 19 and 20 to existing models

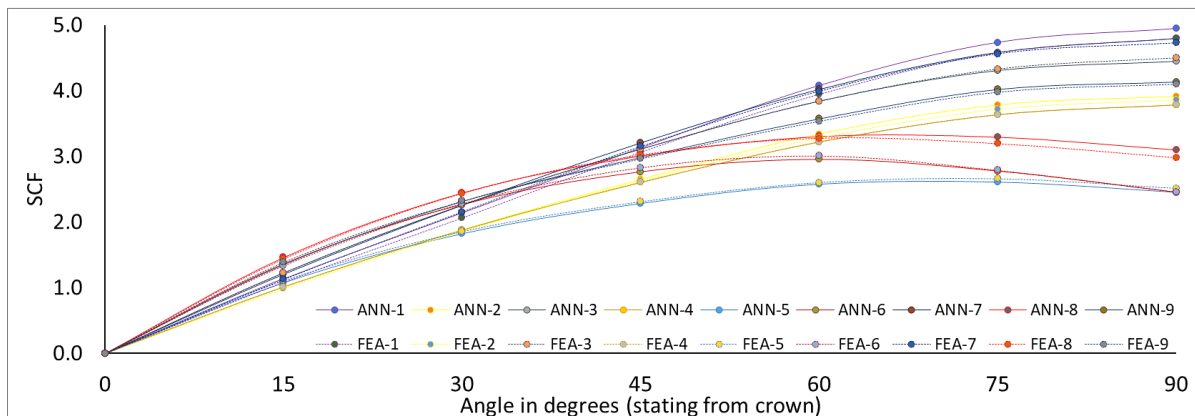


Figure 15. Comparison of stress concentration factor for out-of-plane bending condition-2 determined using empirical model and finite element analysis

Table 3. Details of KT-joints used for validation of empirical models

Design #	Geometric parameters						Dimensionless parameters					
	D	T	L/2	d	t	L	β	γ	τ	Θ	α	ζ
1	200	6	1000	100	4	2000	0.50	16.67	0.67	40.00	20.00	0.50
2	225	7.5	1200	120	4.5	2400	0.53	15.00	0.60	50.00	21.33	0.44
3	250	8	1150	130	5.5	2300	0.52	15.63	0.69	55.00	18.40	0.40
4	300	10	1300	133	6	2600	0.44	15.00	0.60	45.00	17.33	0.33
5	320	8	1350	250	4	2700	0.78	20.00	0.50	35.00	16.88	0.31
6	350	9	1400	280	5.5	2800	0.80	19.44	0.61	50.00	16.00	0.29
7	220	6	1100	90	4	2200	0.41	18.33	0.67	70.00	20.00	0.45
8	320	8	1200	240	5	2400	0.75	20.00	0.63	65.00	15.00	0.31
9	380	10	1300	250	6	2600	0.66	19.00	0.60	35.00	13.68	0.26
Min	200.00	6.00	900.00	90.00	4.00	1800.00	0.41	15.00	0.45	30.00	10.00	0.26
Max	380.00	10.00	1400.00	280.00	6.00	2800.00	0.80	20.00	0.69	70.00	21.33	0.50

The developed empirical models were validated with the literature as well. Efthymiou [9] proposed Equation 11 for determining SCF at the crown in the joint under IPB_C1 and IPB_C2. Similarly, Efthymiou [9] presented Equation 12 for determining SCF at the saddle in the joint under OPB_C1, while OPB_C2 was not covered. Ahmadi & Ali [22] have proposed Equations 13 and 14 for determining SCF at the crown joint under IPB_C1 and IPB_C2, respectively.

4.1. IPB_C1

When the randomly selected KT-joints were subjected to IPB condition-1, according to Figure 1, the peak SCF occurred at the crown position. The SCF determined using the developed empirical models, given as Equations 15 and 16 for IPB_C1, was in good agreement with the FE results, as shown in Figure 9. The difference was less than 5 percent. These equations were extracted from the best epoch of the trained ANN model and validated with equations available in the literature [9, 22] as well, as shown in Figure 10. A good agreement was observed with Efthymiou [9] (less than 6% difference). However, the difference was slightly higher (35–43%) when the SCF determined through the empirical models of this study was compared to the one calculated using the equations proposed by Ahmadi & Ali [22]. The large difference could be due to the limited number of simulations used to extract numerous equations, i.e., only 46 simulations were used to develop ten parametric equations for different IPB load configurations [22].

4.2. IPB_C2

Similar to IPB_C1, the KT-joint under IPB_C2 has a peak SCF at the crown region. Equations 17 and 18 approximate the SCF behavior and are compared with FE model results, as shown in Figure 11. The difference was less than 5%. The position of peak SCF has minor deviations from the crown position, depending on the geometry of the joint. These empirical models were validated with existing equations [9, 22], as shown in Figure 12. The difference was less than 25 percent, which is a bit large but can be considered acceptable, as various critical details regarding the definition of joint geometry are missing in the literature. This comparison imparts confidence in the developed empirical models, which represent a trend similar to that in the literature. Future experimental validation will be beneficial to resolve such discrepancies.

4.3. OPB_C1

The design data set of 929 FE models was simulated under OPB-condition-1, and empirical models were developed and given as Equations 19 and 20. These models were validated by comparing the SCF generated through these models to those generated through detailed FE simulations. A good agreement was observed with a less than 4% difference, as shown in Figure 13. These empirical models were validated with existing equations [9], with less than 15% difference, as shown in Figure 14.

$$\begin{bmatrix} h_1 \\ h_2 \\ h_3 \\ h_4 \\ h_5 \\ h_6 \\ h_7 \\ h_8 \end{bmatrix} = \begin{bmatrix} -0.62 & -0.14 & -0.22 & -0.04 & -0.03 & 0.06 \\ -0.41 & -0.16 & -0.28 & -0.01 & -0.01 & 0.09 \\ -0.75 & -0.35 & -0.36 & -0.04 & 0.14 & 0.29 \\ -0.13 & -0.18 & 0.43 & -0.01 & 0.05 & 0.05 \\ -0.52 & -0.19 & -0.10 & -0.02 & 0.06 & 0.27 \\ -0.07 & -0.20 & -0.39 & 0.66 & 0.14 & -0.02 \\ 0.94 & 0.08 & -0.34 & -0.03 & -0.09 & -0.17 \\ 0.14 & 0.03 & -0.25 & 0.00 & -0.03 & -0.05 \\ 1.03 & 0.18 & -0.40 & -0.01 & -0.10 & -0.20 \\ 0.51 & 0.46 & 0.52 & 0.19 & -2.85 & -0.11 \end{bmatrix} \begin{bmatrix} \beta_n \\ \gamma_n \\ \tau_n \\ \Theta_n \\ \alpha_n \\ \zeta_n \end{bmatrix} + \begin{bmatrix} 1.49 \\ 0.85 \\ 2.21 \\ -0.78 \\ -0.22 \\ 2.45 \\ 1.49 \\ 0.66 \\ 1.64 \\ -3.71 \end{bmatrix} \tag{19}$$

$$\begin{bmatrix} SCF_0 \\ SCF_{15} \\ SCF_{30} \\ SCF_{45} \\ SCF_{60} \\ SCF_{75} \end{bmatrix} = \begin{bmatrix} 4.21 & -0.73 & -3.12 & -0.55 & 0.20 & 0.15 & -1.96 & -2.39 & 1.48 & 0.37 \\ -2.61 & 5.44 & -3.18 & 0.18 & -0.88 & -1.07 & -4.17 & -3.37 & 4.15 & 0.15 \\ 1.99 & 0.96 & -0.81 & -1.67 & -0.91 & 0.22 & -1.62 & -6.63 & 2.27 & 0.01 \\ 3.28 & -1.72 & -0.73 & -2.81 & -0.62 & 1.03 & 1.61 & -7.45 & -0.58 & -0.14 \\ 3.55 & -2.50 & -1.11 & -2.77 & -0.38 & 1.17 & 2.62 & -6.34 & -1.70 & -0.21 \\ 4.23 & -2.89 & -1.30 & -2.71 & -0.30 & 1.31 & 2.90 & -5.95 & -2.03 & -0.23 \end{bmatrix} \begin{bmatrix} h_1 \\ h_2 \\ h_3 \\ h_4 \\ h_5 \\ h_6 \\ h_7 \\ h_8 \end{bmatrix} + \begin{bmatrix} 1.30 \\ 4.68 \\ -0.02 \\ -0.79 \\ -0.87 \\ -1.34 \end{bmatrix} \quad (20)$$

4.4. OPB_C2

Various KT-joints were simulated, and empirical models were developed for OPB_C2. These empirical models are given as Equations 21 and 22. These models were validated through random KT-joints in Table 3. The difference was less than 4% for SCF determined empirically compared to the FEA simulation results, as shown in Figure 15. Equations were unavailable in the literature for validation.

$$\begin{bmatrix} h_1 \\ h_2 \\ h_3 \\ h_4 \\ h_5 \\ h_6 \end{bmatrix} = \begin{bmatrix} -0.58 & -0.10 & -0.27 & 0.00 & 0.15 & 0.02 \\ -0.27 & -0.12 & -0.22 & 0.09 & 0.33 & 0.01 \\ 0.02 & -0.09 & -0.22 & 0.00 & 0.04 & 0.04 \\ 1.10 & 0.07 & -0.52 & -0.55 & -1.45 & -0.27 \\ 0.13 & 0.05 & -0.01 & 0.26 & -0.16 & 0.01 \\ -0.21 & 0.13 & 0.02 & 0.01 & -0.06 & 0.02 \\ -0.46 & 0.13 & 0.03 & -0.02 & -0.06 & 0.18 \\ 0.04 & 0.03 & -0.03 & 0.34 & -0.06 & 0.02 \\ -0.41 & -0.10 & -0.09 & -0.09 & 0.24 & 0.13 \\ -0.37 & -0.17 & 0.45 & -0.01 & -0.01 & -0.01 \end{bmatrix} \begin{bmatrix} \beta_n \\ \gamma_n \\ \tau_n \\ \theta_n \\ \alpha_n \\ \zeta_n \end{bmatrix} + \begin{bmatrix} 1.90 \\ 1.67 \\ 0.57 \\ -1.33 \\ 0.29 \\ -0.61 \\ -0.38 \\ 0.13 \\ -0.71 \\ -1.30 \end{bmatrix} \quad (21)$$

$$\begin{bmatrix} SCF_{15} \\ SCF_{30} \\ SCF_{45} \\ SCF_{60} \\ SCF_{75} \\ SCF_{90} \end{bmatrix} = \begin{bmatrix} 1.84 & 2.89 & -6.38 & -0.11 & 4.14 & -0.88 & -0.87 & -2.61 & 2.32 & -1.53 \\ 1.72 & 3.21 & -6.52 & -0.06 & 2.66 & -1.86 & -0.15 & -1.67 & 1.42 & -1.46 \\ 2.05 & 1.23 & -6.29 & 0.03 & -1.04 & -3.69 & 1.31 & 0.77 & -0.31 & -1.63 \\ 3.01 & -2.44 & -4.60 & 0.10 & -5.17 & -4.71 & 2.45 & 3.48 & -2.21 & -1.59 \\ 4.71 & -5.42 & -3.61 & 0.15 & -7.29 & -4.81 & 2.78 & 4.94 & -2.96 & -1.58 \\ 5.85 & -6.48 & -3.31 & 0.16 & -7.61 & -4.61 & 2.71 & 5.20 & -2.98 & -1.53 \end{bmatrix} \begin{bmatrix} h_1 \\ h_2 \\ h_3 \\ h_4 \\ h_5 \\ h_6 \end{bmatrix} + \begin{bmatrix} -3.06 \\ -3.50 \\ -2.90 \\ -1.60 \\ -0.88 \\ -0.96 \end{bmatrix} \quad (22)$$

5. Computation of Hot-Spot Stress Using Empirical Equations

Fatigue life estimation using S-N curves requires the peak HSS of a tubular joint based on the load condition. The empirical models were used to compute HSS around the chord-central brace interface of KT-joint subjected to different bending load configurations, using the approach by Ahmadi & Ali [22]. A MATLAB code yielding HSS for 0°-360° of the chord-brace interface was developed, with dimensionless parameters (β, γ, τ, θ, α, ζ) and magnitude for IPB and OPB loads as input. This plot identifies the peak HSS along the weld toe for fatigue life estimation using the S-N curve. This method can be used to determine peak HSS along the weld toe of the brace/chord interface, including the crown and saddle.

5.1. Individual Bending Load

The codes can be used for KT-joint under any bending loads. If the joint is subjected to IPB or OPB, the other load will be zero. Figure 16 compares the HSS calculated with the empirical equations for individual bending loads. The error in the computed peak HSS is less than 0.8%. Table 4 lists the error in peak HSS for various bending combinations.

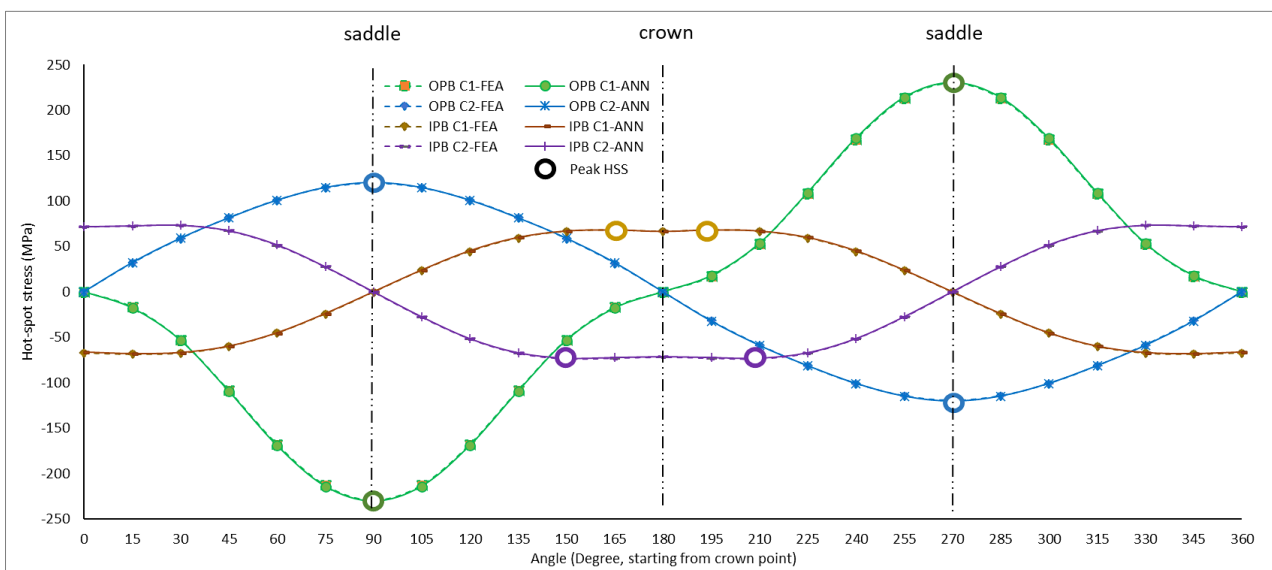


Figure 16. Hot-spot stress due to individual bending loads (30 MPa) on all braces of KT-joint

Table 4. Peak HSS position and error for various bending loads

Load Type	Load case	Position of peak HSS	% Error in peak HSS
Individual bending load (uniplanar)	IPB_C1	15° from crown	0.2
	IPB_C2	30° from crown	0.2
	OPB_C1	saddle (90° from crown)	0.4
	OPB_C2	saddle (90° from crown)	0.8
Simultaneous bending loads (multiplanar)	IPB_C1 + OPB_C1 4:1	60° from crown	1.4
	IPB_C1 + OPB_C1 2:1	75° from crown	0.7
	IPB_C1 + OPB_C1 1:1	75° from crown	0.6
	IPB_C1 + OPB_C1 1:2	saddle (90° from crown)	0.4
	IPB_C1 + OPB_C1 1:4	saddle (90° from crown)	0.4
	IPB_C1 + OPB_C2 4:1	30° from crown	0.3
	IPB_C1 + OPB_C2 2:1	45° from crown	0.3
	IPB_C1 + OPB_C2 1:1	60° from crown	0.1
	IPB_C1 + OPB_C2 1:2	75° from crown	0.3
	IPB_C1 + OPB_C2 1:4	75° from crown	0.3
	IPB_C2 + OPB_C2 4:1	30° from crown	0
	IPB_C2 + OPB_C2 2:1	45° from crown	0.1
	IPB_C2 + OPB_C2 1:1	60° from crown	0.3
	IPB_C2 + OPB_C2 1:2	75° from crown	0.3
IPB_C2 + OPB_C2 1:4	75° from crown	0.3	

5.2. Combined Bending Load

When bending at an angle to the orthogonal axis of the joint, the peak HSS occurs between the crown and saddle points [26]. A KT-joint was simulated for different combinations of combined bending to show this shift and as a proof of concept of the empirical models to determine peak HSS in such scenarios. Table 4 summarizes these loads and the positions of peak HSS. The three possible bending configurations are presented in the following sections:

5.2.1. IPB_C1 + OPB_C1

KT-joints under different combinations of IPB and OPB were simulated. The simultaneous application of IPB_C1 and OPB_C1 causes variation in the position of peak HSS, as shown in Figure 17.

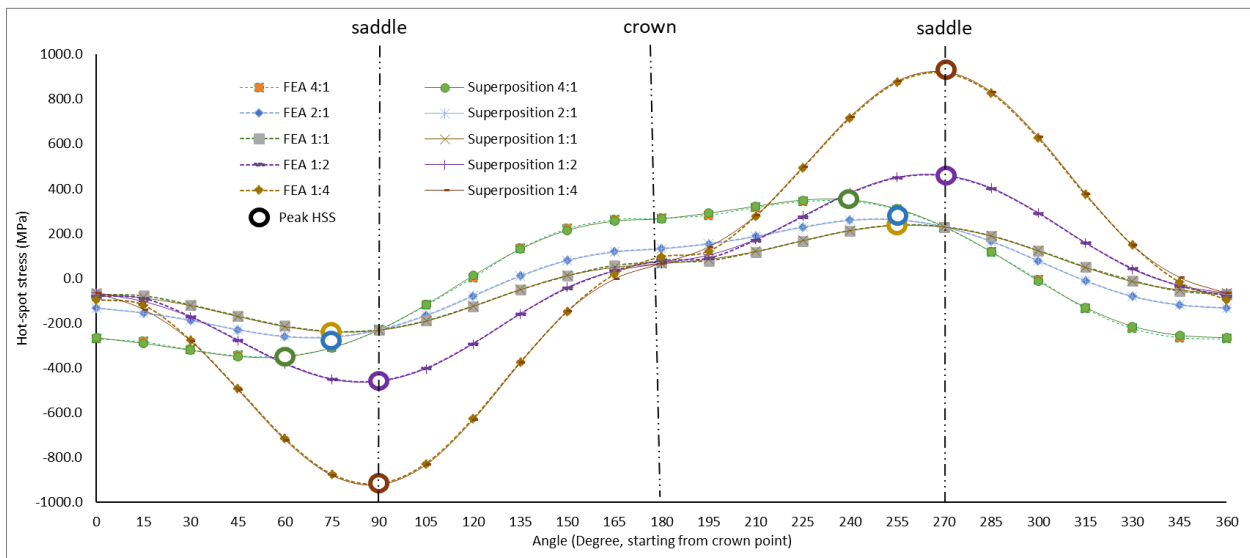


Figure 17. Comparison of hot-spot stress for simultaneous in-plane bending condition-1 and out-of-plane bending condition-1 determined using empirical models and finite element analysis

IPB and OPB ratios of 4:1, 2:1, 1:1, 1:2, and 1:4 were used, with "1" representing a 30 MPa bending stress. Equations 20–23 were used for SCF calculation, and combined HSS was calculated using Equation 10. When an IPB_C1 load of 30 MPa was applied with an OPB_C1 load of 30, 60, and 120 MPa, the peak HSS was at 75° from the crown (15° from the saddle) and remained at the saddle for the following two load combinations. When OPB_C1 magnitude was fixed

and IPB_C1 was varied, the peak HSS was at 75°, 75°, and 60° from the crown. The variation in peak HSS position emphasizes the need for empirical models capable of determining SCF around the axis. If hot-spot stress lower than peak HSS is selected, as would be the case if the equations from the literature were used, it will result in an unrealistic high fatigue life estimation through the respective S-N curve. These findings were validated with detailed FEA and a maximum of 1.4% error at the peak HSS points, as listed in Table 4.

5.2.2. IPB_C1 + OPB_C2

The second load configuration was IPB_C1 and OPB_C2. The same five load cases were simulated, i.e., 4:1, 2:1, 1:1, 1:2, and 1:4 (1 being 30 MPa). For equal magnitudes of IPB_C1 and OPB_C2, the peak HSS was 60° from the crown point. When the magnitude of IPB_C1 was doubled, the peak HSS was at the 45° position. When the IPB_C1 was further increased, the peak was 30° from the crown. Similarly, with IPB_C1 fixed, three magnitudes of OPB_C2 were applied to determine the variation in the position of peak HSS. The peak HSS was 60° from the crown for the same load and 15° from the crown for the following two load cases. The maximum difference was 0.3% compared to the FEA simulation results, as shown in Figure 18.

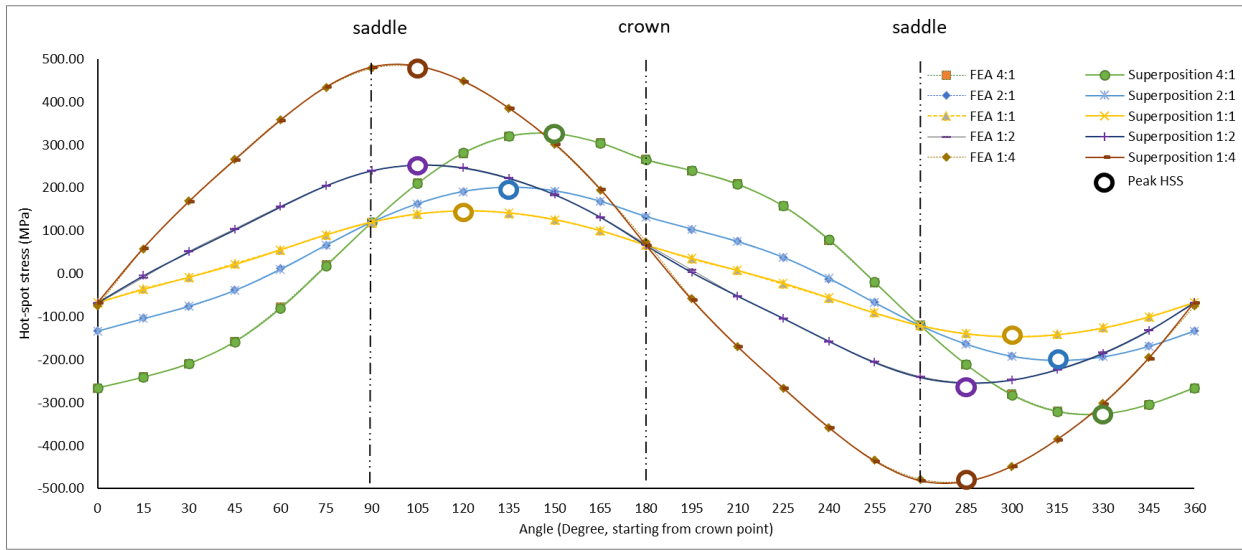


Figure 18. Comparison of hot-spot stress for simultaneous in-plane bending condition-1 and out-of-plane bending condition-2 determined using empirical models and finite element analysis

5.2.3. IPB_C2 + OPB_C2

The last combination was IPB_C2 and OPB_C2. The peak HSS occurred at 60°, 45°, and 30° from the crown when IPB_C2 of 30 MPa was applied with OPB_C2 of 30, 60, and 120 MPa bending stress. The peak HSS occurred at 60°, 75°, and 75° from the crown when 30 MPa OPB_C2 was applied with IPB_C2 of 30, 60, and 120 MPa stress. A similar trend was found for peak HSS based on the equations, with a maximum error of 0.3%, as shown in Figure 19.

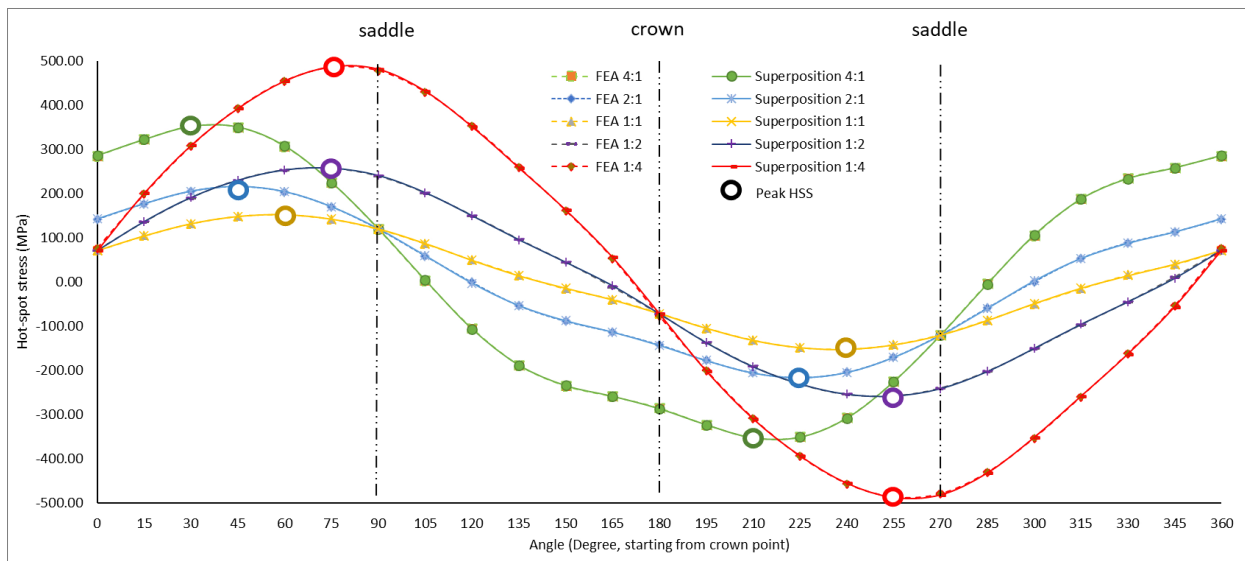


Figure 19. Comparison of hot-spot stress for simultaneous in-plane bending condition-2 and out-of-plane bending condition-2 determined using empirical models and finite element analysis

6. Conclusion

Existing models estimate peak hot-spot stress (HSS) at the crown or saddle. However, for a KT-joint under multiplanar loads, the peak HSS could occur anywhere along the weld toe of the brace-chord interface, which can be significantly higher than the HSS observed at the crown or saddle. As such, fatigue life can be overestimated if the HSS at the crown or saddle is used for fatigue analysis of the KT-joint under multiplanar bending. This study investigated the stress concentration factor (SCF) and HSS in KT-joints under multiplanar bending, addressing the limitations of existing models by proposing new empirical models to predict SCF and HSS with exceptional accuracy. Various KT-joint designs were generated, and 3716 simulations were performed. The HSS at the weld toe at 24 equidistant positions around the brace axis was determined based on the linear extrapolation of maximum principle stress. The HSS was expressed as a SCF at the weld toe. Artificial neural networks were trained using the simulation data, employing dimensionless joint parameters as input and SCF as output. Subsequently, empirical equations were developed to predict peak HSS for any combination of bending loads with less than 1.5% error. It was highlighted that the difference in HSS at the crown or saddle and the peak HSS depends on the relative magnitudes of in-plane and out-of-plane bending loads. These models may be validated experimentally in the future to enhance their reliability. Additionally, similar models could be developed for different joint types and load conditions using similar methodologies.

7. Abbreviations and Symbols

API	American Petroleum Institute	β	d/D
ANN	Artificial neural networks	γ	$D/2T$
DoE	Design of Experiment	τ	t/T
FE	Finite element	α	$2L/D$
FEA	Finite element analysis	ζ	g/D
FEM	Finite element method	ip_x	Input to ANN
HSS	Hot spot stress, the maximum principal stress extrapolated at the weld toe	hn_x	Output of a hidden layer
IPB	In-plane bending moment	W_x	Weight of a neuron
SCF	Stress concentration factor	B_x	Bias of a layer
OPB	Out-of-plane bending moment	$i_{n,max}$	The upper range of normalized input data
Peak HSS	Maximum value of hot-spot stress (HSS) around the brace axis	$i_{n,min}$	The lower range of normalized input data
θ	Angle of the inclined brace with chord axis	i_{max}	Maximum of dimensionless input data
D	Diameter of the chord	i_{min}	Minimum of dimensionless input data
d	Diameter of the brace (all braces kept same)	$o_{n,max}$	The upper range of normalized output data
T	Thickness of the chord	$o_{n,min}$	The lower range of normalized output data
t	The thickness of the brace (all braces kept the same)	o_{max}	Maximum SCF input used for ANN training
g	The gap between the central and inclined brace	o_{min}	Minimum SCF input used for ANN training
σ_n	Nominal stress		

8. Declarations

8.1. Author Contributions

Conceptualization, S.K. and M.I.; methodology, M.I. and A.K.; software, M.I. and M.F.; validation, M.I.; formal analysis, M.I.; investigation, M.I.; resources, S.K.; data curation, S.K. and M.O.; writing—original draft preparation, M.I.; writing—review and editing, M.I. and M.O.; visualization, M.I.; supervision, S.K., V.P., and M.O.; project administration, S.K. and V.P.; funding acquisition, S.K. All authors have read and agreed to the published version of the manuscript.

8.2. Data Availability Statement

The data presented in this study are available on request from the corresponding author.

8.3. Funding

This research received funding from Yayasan Universiti Teknologi PETRONAS under Grant No 015LC0-443.

8.4. Conflicts of Interest

The authors declare no conflict of interest.

9. References

- [1] Vieira Ávila, B., Correia, J., Carvalho, H., Fantuzzi, N., De Jesus, A., & Berto, F. (2022). Numerical analysis and discussion on the hot-spot stress concept applied to welded tubular KT joints. *Engineering Failure Analysis*, 135. doi:10.1016/j.engfailanal.2022.106092.
- [2] Zhou, K., Zuo, J., Wang, W., & Bao, S. (2020). Stress Concentration Factors for Multi-planar Tubular Joints Subjected to Axial Loading. *E3S Web of Conferences*, 213. doi:10.1051/e3sconf/202021303014.
- [3] Iqbal, M., Karuppanan, S., Perumal, V., Ovinis, M., & Rasul, A. (2023). Rehabilitation Techniques for Offshore Tubular Joints. *Journal of Marine Science and Engineering*, 11(2), 461. doi:10.3390/jmse11020461.
- [4] Maheswaran, J., & Siriwardane, S. C. (2016). Fatigue life estimation of tubular joints - A comparative study. *Fatigue & Fracture of Engineering Materials & Structures*, 39(1), 30–46. doi:10.1111/ffe.12314.
- [5] Hoon, K. H., Wong, L. K., & Soh, A. K. (2001). Experimental investigation of a doubler-plate reinforced tubular T-joint subjected to combined loadings. *Journal of Constructional Steel Research*, 57(9), 1015–1039. doi:10.1016/S0143-974X(01)00023-2.
- [6] Kuang, J. G., Potvin, A. B., & Leick, R. D. (1975). Stress concentration in tubular joints. *Proceedings of the Annual Offshore Technology Conference*, doi:10.4043/2205-MS.
- [7] Wordsworth, A.C. (1981). *Stress Concentration Factors at K and KT tubular joints*. Fatigue in Offshore Structural Steels, Thomas Telford Publishing, London, United Kingdom.
- [8] Wordsworth, A. C., & Smedley, G. P. (1978). Stress concentrations at unstiffened tubular joints. *European Offshore Steels Research Seminar*, 27-29 November, 1978, Abington Hall, United Kingdom.
- [9] Efthymiou, M. (1988). Development of SCF formulae and generalized influence functions for use in fatigue analysis. OTJ 88. *Recent Developments in Tubular Joints Technology*, Surrey, United Kingdom.
- [10] Hellier, A. K., Connolly, M. P., & Dover, W. D. (1990). Stress concentration factors for tubular Y- and T-joints. *International Journal of Fatigue*, 12(1), 13–23. doi:10.1016/0142-1123(90)90338-F.
- [11] Lloyd's Register. (1992). *Stress Concentration Factors for Tubular Complex Joints*, Lloyd's Register of Shipping for health and Safety Executive, Offshore Technology Report, (OTH 91 353), 1-106.
- [12] Smedley, P., & Fisher, P. (1991). Stress concentration factors for simple tubular joints. *International Ocean and Polar Engineering Conference (ISOPE)*, 11-16 August, 1991, Edinburgh, United Kingdom.
- [13] Morgan, M. R., & Lee, M. M. K. (1997). New parametric equations for stress concentration factors in tubular K-joints under balanced axial loading. *International Journal of Fatigue*, 19(4), 309–317. doi:10.1016/S0142-1123(96)00081-3.
- [14] Morgan, M. R., & Lee, M. M. K. (1998). Parametric equations for distributions of stress concentration factors in tubular K-joints under out-of-plane moment loading. *International Journal of Fatigue*, 20(6), 449–461. doi:10.1016/S0142-1123(98)00011-5.
- [15] DNV. (2016). *DNVGL-RP-C203. Fatigue design of offshore structures*. DNV, Bærum, Norway.
- [16] Norsok: N-004. (2004). *design of steel structures*. Standards Norway, Oslo, Norway.
- [17] Zhao, X.-L., Herion, S., Packer, JA., Puthli, RS., Sedlacek, G., Wardenier, J., Weynand, K., van Wingerde, AM., & Yeomans, NF. (2000). Design guide for circular and rectangular hollow section welded joints under fatigue loading. In *Design guide for circular and rectangular hollow section welded joints under fatigue loading*, 1-121. TUV-Verlag, Koln, Germany.
- [18] Ahmadi, H., & Zavvar, E. (2015). Stress concentration factors induced by out-of-plane bending loads in ring-stiffened tubular KT-joints of jacket structures. *Thin-Walled Structures*, 91, 82–95. doi:10.1016/j.tws.2015.02.011.
- [19] Ahmadi, H., & Lotfollahi-Yaghin, M. A. (2015). Stress concentration due to in-plane bending (IPB) loads in ring-stiffened tubular KT-joints of offshore structures: Parametric study and design formulation. *Applied Ocean Research*, 51, 54–66. doi:10.1016/j.apor.2015.02.009.
- [20] Ahmadi, H., Yeganeh, A., Mohammadi, A. H., & Zavvar, E. (2016). Probabilistic analysis of stress concentration factors in tubular KT-joints reinforced with internal ring stiffeners under in-plane bending loads. *Thin-Walled Structures*, 99, 58–75. doi:10.1016/j.tws.2015.11.010.
- [21] Ahmadi, H. (2016). A probability distribution model for SCFs in internally ring-stiffened tubular KT-joints of offshore structures subjected to out-of-plane bending loads. *Ocean Engineering*, 116, 184–199. doi:10.1016/j.oceaneng.2016.02.037.
- [22] Ahmadi, H., Ali, Z.N. (2016). Stress Concentration Factors in Uniplanar Tubular KT-Joints of Jacket Structures Subjected to In-Plane Bending Loads, *International Journal of Maritime Technology*, 5, 27-39.
- [23] Ahmadi, H., & Zavvar, E. (2016). The effect of multi-planarity on the SCFs in offshore tubular KT-joints subjected to in-plane and out-of-plane bending loads. *Thin-Walled Structures*, 106, 148–165. doi:10.1016/j.tws.2016.04.020.

- [24] Zavvar, E., Hectors, K., & De Waele, W. (2021). Stress concentration factors of multi-planar tubular KT-joints subjected to in-plane bending moments. *Marine Structures*, 78(March), 103000. doi:10.1016/j.marstruc.2021.103000.
- [25] Zavvar, E., Sadat Hosseini, A., & Lotfollahi-Yaghin, M. A. (2021). Stress concentration factors in steel tubular KT-connections with FRP-Wrapping under bending moments. *Structures*, 33, 4743–4765. doi:10.1016/j.istruc.2021.06.100.
- [26] Iqbal, M., Karuppanan, S., Perumal, V., Ovinis, M., & Nouman, H. (2023). Empirical modeling of stress concentration factors using finite element analysis and artificial neural networks for the fatigue design of tubular KT-joints under combined loading. *Fatigue and Fracture of Engineering Materials and Structures*, 46(11), 4333–4349. doi:10.1111/ffe.14122.
- [27] Yeoh, S. K., Soh, A. K., & Soh, C. K. (1995). Behaviour of tubular T-joints subjected to combined loadings. *Journal of Constructional Steel Research*, 32(3), 259–280. doi:10.1016/0143-974X(95)93898-E.
- [28] Gulati, K. C., Wang, W. J., & Kan, D. K. Y. (1982). An analytical study of stress concentration effects in multibrace joints under combined loading. *Proceedings of the Annual Offshore Technology Conference, OTC-4407-MS*, Texas, United States. doi:10.4043/4407-ms.
- [29] ARSEM. (1987). *Design guides for offshore structures - welded tubular joints*, Vol. 1, Technip, Association de recherche sur les structures métalliques marines (ARSEM), Paris, France.
- [30] American Petroleum Institute (API). (2014). *API Recommended Practice 2A-WSD. Planning, Designing, and Constructing Fixed Offshore Platforms—Working Stress Design*. American Petroleum Institute (API), Washington, United States.
- [31] Ahmadi, H., Lotfollahi-yaghin, M. A., & Yong-bo, S. (2013). Experimental and Numerical Investigation of Geometric SCFs in Internally Ring-Stiffened Tubular KT-Joints of Offshore Structures. *Journal of the Persian Gulf*, 43(1), 7–8.
- [32] Ahmadi, H. (2019). Probabilistic analysis of the DoB in axially-loaded tubular KT-joints of offshore structures. *Applied Ocean Research*, 87, 64–80. doi:10.1016/j.apor.2019.03.018.
- [33] van Wingerde, A. M., Packer, J. A., & Wardenier, J. (1995). Criteria for the fatigue assessment of hollow structural section connections. *Journal of Constructional Steel Research*, 35(1), 71–115. doi:10.1016/0143-974X(94)00030-I.
- [34] N'Diaye, A., Hariri, S., Pluvinage, G., & Azari, Z. (2007). Stress concentration factor analysis for notched welded tubular T-joints. *International Journal of Fatigue*, 29(8), 1554–1570. doi:10.1016/j.ijfatigue.2006.10.030.
- [35] Iqbal, M., Karuppanan, S., Perumal, V., Ovinis, M., & Hina, A. (2023). An Artificial Neural Network Model for the Stress Concentration Factors in KT-Joints Subjected to Axial Compressive Load. *Materials Science Forum*, 1103, 163–175. doi:10.4028/p-ypo50i.
- [36] Vijaya Kumar, S. D., Lo, M., Karuppanan, S., & Ovinis, M. (2022). Empirical Failure Pressure Prediction Equations for Pipelines with Longitudinal Interacting Corrosion Defects Based on Artificial Neural Network. *Journal of Marine Science and Engineering*, 10(6). doi:10.3390/jmse10060764.
- [37] Soh, A. K., & Soh, C. K. (1995). Stress analysis of axially loaded T tubular joints reinforced with doubler plates. *Computers and Structures*, 55(1), 141–149. doi:10.1016/0045-7949(94)00412-V.
- [38] Ahmadi, H., & Zavvar, E. (2020). Degree of bending (DoB) in offshore tubular KT-joints under the axial, in-plane bending (IPB), and out-of-plane bending (OPB) loads. *Applied Ocean Research*, 95(2020), 102015. doi:10.1016/j.apor.2019.102015.